

All Optical Echo State Network Reservoir Computing

Ishwar S. Kaushik*, Peter J. Ehlers, and Daniel Soh†
Wyant College of Optical Sciences, University of Arizona, Tucson, Arizona, USA
(Dated: September 16, 2025)

We propose an innovative design for an all-optical Echo State Network (ESN), an advanced type of reservoir computer known for its universal computational capabilities. Our design enables fully optical implementation of arbitrary ESNs, featuring flexibility in optical matrix multiplication and nonlinear activation. Leveraging the nonlinear characteristics of stimulated Brillouin scattering (SBS), the architecture efficiently realizes measurement-free nonlinear activation. The approach significantly reduces computational overhead and energy consumption compared to traditional software-based methods. Comprehensive simulations validate the system’s memory capacity, nonlinear processing strength, and polynomial algebra capabilities, showcasing performance comparable to software ESNs across key benchmark tasks. Our design establishes a feasible, scalable, and universally applicable framework for optical reservoir computing, suitable for diverse machine learning applications.

I. INTRODUCTION

Recurrent neural networks (RNNs) have inherent memory capabilities, and are trained on sequential or time series data to create a machine learning model that attempts to make accurate time series predictions [1]. However, their reliance on multiple layers of tunable weights leads to high computational and training costs. A potential way to overcome this cost is with a recent paradigm of RNNs with fixed internal weights, known as reservoir computers (RCs). Reservoir computing has been of recent interest, with applications to time-series prediction tasks, classification tasks, and much more [2–12]. Unlike RNNs, which require large amounts of time and resources, RCs offer a much less computationally expensive method for machine learning.

An RC is a nonlinear dynamical system driven by time-dependent inputs and a single trainable output layer. Unlike RNNs or deep learning architectures, the inner layers of the computing reservoir are fixed and all of the training takes place in the final output layer. This output is usually a simple linear combination of the values of the state-vector of the reservoir, which allows for the weights to be determined by simple linear regression. This property makes reservoir computing an attractive choice for hardware designs; manipulating the weights in multiple layers for a typical RNN in hardware is exceedingly difficult in comparison to this simpler approach. Moreover, by adopting a lean, hardware-centric design in RCs, the overall hardware overhead is significantly reduced compared to software-based systems that depend on traditional computing layers—such as CPUs, long-term and short-term memories, and their interconnects. Operating on specialized hardware further increases speed by eliminating unnecessary data processing steps, thus improving overall efficiency.

Optical platforms for computation and machine learning can, in principle, achieve more efficient computation in terms of energy and time [13, 14]. One important challenge in all-optical approaches is how to realize the nonlinear activation. For this, various nonlinear optical processes have been studied including the nonlinear behavior of SBS [15]. It is important to note that, while the implementations of all-optical reservoir computers have been reported [16], the realization of an all-optical RC with universal computation capability (i.e., universality) has not yet been demonstrated to our best knowledge.

Universality refers to a computing machine’s ability to perform any computational task with any desired accuracy. In a supervised learning context, it specifically denotes the capacity to approximate any input-output relationship with arbitrary precision. Consequently, having a mathematically rigorous proof of universality is very desirable, as it ensures that the computing scheme can robustly handle a wide range of tasks. Arbitrary RCs are not guaranteed to obey the conditions necessary to be capable of universal computations. We present, for the first time to our best knowledge, a new approach representing a novel all-optical implementation of Echo State Networks (ESNs), which have recently been shown to form a universal approximating class of RCs [17].

ESNs are a family of RCs that are formed from iteratively applying a nonlinear transformation after a fixed linear transformation applied at each input time step [18]. ESNs are similar to RNNs except that the linear weights given to the state of the system at each time step are fixed for the entire run. The family of ESNs as a whole is universal [17] which means that for a given target sequence and input, we can find a specific ESN configuration that can approximate the target function to any desired accuracy.

Here, we propose an innovative way to realize an all-optical implementation of any desired ESN configuration. The advantages provided by an all-optical reservoir architecture, as stated earlier, are fast computation and better energy efficiency than large software alternatives. For this reason, there has been growing interest in re-

* Contact author: ishwarikaushik@arizona.edu

† Contact author: danielsoh@arizona.edu

cent years in optical implementations of the matrix multiplication stage of machine learning architectures [19–21]. Here, we propose an in-fiber method for optical matrix-vector multiplication, which is followed by an in-fiber solution for optical nonlinear activation inspired by Slinkov et. al [22] using SBS. This unique combination of measurement-free matrix multiplication and nonlinear activation allows for a feasible design of the optical ESN.

The paper is organized as follows: Section II covers the basic concepts of ESNs and the theory behind the SBS linear amplifiers and activation function, Section III addresses our proposed design for the all-optical ESN, and Section IV compiles the performance of the ESN on various tasks that evaluate its universality, and compares it to a software ESN of the same size. The tunability of the nonlinearity of SBS interaction is also analyzed in this section. Finally, Section V contains the concluding remarks.

II. OPTICAL RESERVOIR COMPUTING CONCEPTS

A. Echo State Network

An ESN is a form of reservoir computing, responding to time-series inputs reflected in its state vector after each time step. The state of the reservoir at each time step is given by

$$x_{k+1} = g(x_k, u_k). \quad (1)$$

Where the vector x_k represents the state of the reservoir at time step k . The number of elements of the state vector is equal to the number of nodes N of the reservoir computer. The function $g(x_k, u_k)$ is a fixed nonlinear function of the reservoir that provides the updated state of the reservoir dependent on the k th element of the input sequence u_k . The predicted output of the network is given by

$$\hat{y}_k = W^T x_k + C, \quad (2)$$

and the cost function is

$$S = \frac{1}{2N} \sum_{k=0}^{N-1} (y_k - \hat{y}_k)^2. \quad (3)$$

The parameters W and C given in Equation (2) are chosen to minimize the cost function S given in Equation (3). Here, y_k denotes the target sequence the network output is fit to. So, the fitting of the output function to the target data is a linear regression problem. The reservoir dynamics are a nonlinear function of the inputs u_k . The readouts from the reservoir can be used to approximate the function y_k with linear regression.

A reservoir computer is required to satisfy the uniform convergence property [17]. This property asserts that the reservoir state converges to a unique sequence after many time steps, which means that the initial state of the reservoir from the distant past has no effect on the current state. This property can be extended by including the continuity of $g(x_k, u_k)$ and result in the fading memory property [23]. The fading memory property implies that the dependence of the state vector of the reservoir x_k on the input u_{k_0} at a time step k_0 must diminish as $k - k_0$ tends to infinity. This allows for a universal, repeatable, and deterministic reservoir while still maintaining some memory.

An ESN [18] is a type of reservoir computer with a form given by

$$g(x_k, u_k) = f(Ax_k + Bu_k), \quad (4)$$

where A is a random but fixed matrix and B is a random, fixed vector. The function $f(z)$ is a nonlinear activation function that acts on the input $z = Ax_k + Bu_k$. For N nodes of the reservoir, the matrix A has dimensions $N \times N$ and the vector B has dimensions $N \times 1$. Uniform convergence of an ESN is guaranteed by the condition that $A^T A < a^2 I_n$ where a is a number determined by the nonlinear function $f(z)$ [24]. Hence, the fading memory property is also guaranteed for a stable ESN, which leads to the universal approximation capability of this class of reservoir computers.

B. Nonlinear Activation Mechanism

SBS is a third-order nonlinear scattering process. The optical pump wave interacts with the acoustic wave of the medium, which is stimulated by the presence of the pump and probe waves. This interaction amplifies the probe wave by depleting the pump. Writing the SBS interaction in terms of coupled powers of the pump and probe optical waves [25], we have

$$\frac{dP_p}{dz} = -gP_pP_s, \quad (5)$$

$$-\frac{dP_s}{dz} = +gP_sP_p. \quad (6)$$

Equations (5) and (6) show the coupled power relations with propagation distance. The pump wave is represented by P_p and the probe wave is represented by P_s . The SBS gain factor g is known in terms of the Brillouin frequency, Brillouin linewidth, and other material properties of the medium like the refractive index. Solving Equations (5) and (6), we get a transcendental equation in terms of P_{out} given by (see the derivation in Appendix A)

$$P_{\text{out}}(P_{\text{in}} + P_p - P_{\text{out}}) - P_{\text{in}}P_p e^{-(P_p - P_{\text{out}})gL} = 0. \quad (7)$$

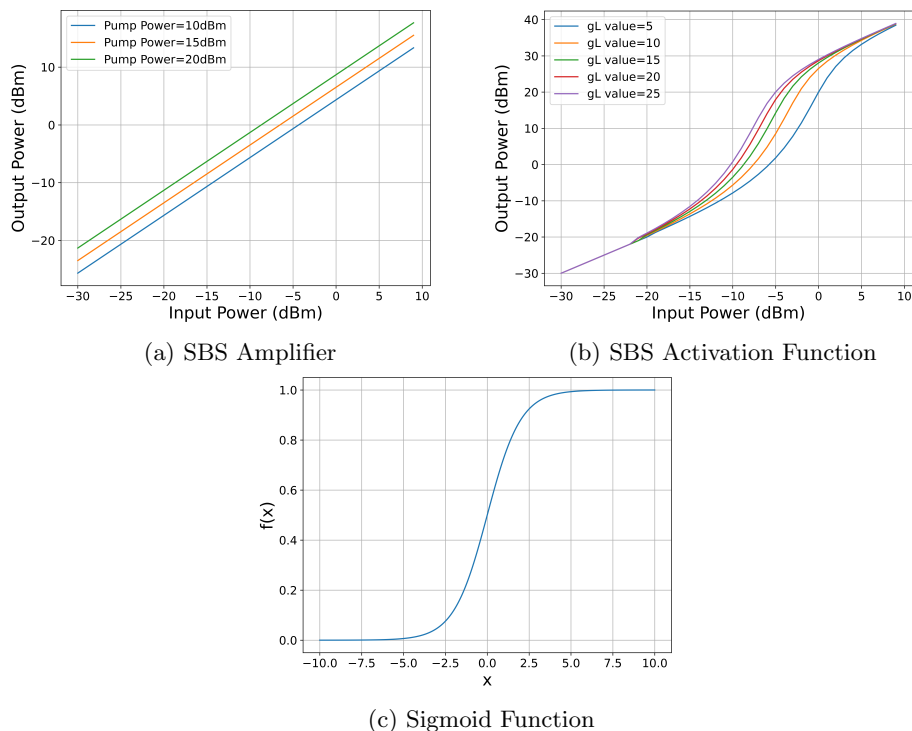


FIG. 1: (a) SBS operating in large pump (linear) regime. Input-output relationship is shown for various pump powers to demonstrate tunability. (b) SBS operating in self-pumped (nonlinear) regime. The nonlinear shape can be designed by choosing an appropriate gL value. (c) Sigmoid function for comparison.

We have defined $P_s(L) = P_{\text{out}}$. We also define $P_s(0) = P_{\text{in}}$. Here, L is the length of SBS interaction. Equation (7) does not have an analytical solution but is solved approximately using numerical methods. Within the large pump approximation, which means that the pump power is much larger than the probe, the solution is linear and controlled by the pump power. When the pump power is made dependent on the input power the solution is nonlinear as shown by Slinkov et. al [22]. By amplifying and splitting the input with an appropriate ratio, we are able to optimize the nonlinear activation. We use these two behaviors to encode matrix multiplications and nonlinear activation in the optical ESN implementation.

The behavior of the transcendental Equation (7) has been simulated numerically, and is shown in Figure 1. Particularly, the nonlinear behavior of SBS looks very similar to a sigmoid function, which is often used as an activation function for machine learning applications. The sigmoid function is plotted for comparison in Figure 1(c). The linear behavior is tunable by varying the pump power and the nonlinear regime shows different behavior for different values of the gL product given in the exponent of Equation (7), and also for different values of the pump splitting ratio. This allows for an optimizable activation function, which we expand on later in the paper.

III. OPTICAL ESN MODEL

The optical ESN model is shown in Figure 2. It is designed in an all-fiber platform to make use of highly nonlinear fiber-based SBS for the all-optical activation function. According to the governing Equation (4), the design goal is to implement a matrix-vector multiplication followed by nonlinear activation.

The architecture aims to physically realize the ESN update Equation (1) at each time step by sequentially performing matrix-vector multiplications followed by nonlinear activation Equation (4). As shown in Figure 2, the input u_k is encoded by a variable attenuator (VOA) at each time step k . The required B' vector elements are encoded using Brillouin amplifiers with appropriately tuned pump powers according to Equation (7) operating in the large pump regime, which gives a linear input-output relation as shown in Figure 1. The vector B' is chosen such that $AB' = B$ to satisfy the ESN design in Equation (4). The values of the A matrix are realized with a combination of a VOA and a Brillouin amplifier. This allows access to arbitrary (positive or negative) matrix elements, as discussed further below.

The input vector is combined with the optical reservoir using fiber beam combiners. These are coherent optical beam combiners, which introduces the possibility of reduced performance due to phase fluctuations. Fiber systems are known to have phase fluctuations due to vibra-

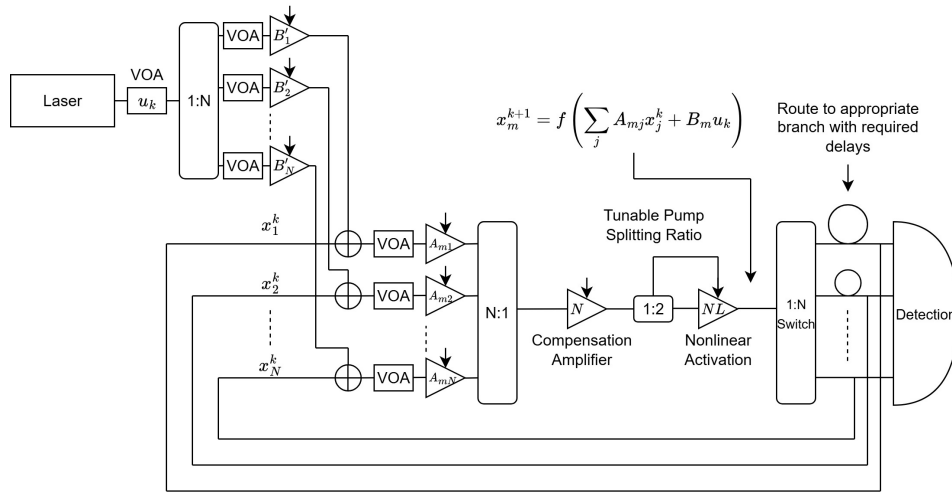


FIG. 2: All Optical ESN Design

tions, which necessitates the use of a phase lock loop to ensure coherent operation of the beam combiners. Electronic servo systems, such as the system proposed by Liang et al. [26] can be used to mitigate this issue.

The matrix multiplication is performed in a series of sub-steps that each time step k is divided into. Each sub-step is denoted by the index m , and represents multiplication of the elements of the x_k vector with each successive row of the matrix A . These multiplications are performed by appropriately tuning the array of VOAs for the inputs and the pump powers in the array of Brillouin amplifiers. As these amplifiers must be modulated every sub-step, the pump powers are also controlled by VOAs. We allow for negative elements in the ESN design matrices by representing the values of the state vector in dBm units.

While the Brillouin amplifiers implement only positive multiplication values (as the operation takes place in units of W), the accompanying VOAs can be tuned in each sub-step to achieve the desired negative value at the output in dBm units. This allows us to access negative matrix elements by using the appropriate range of optical powers below 0 dBm. Thus, we realized the ESN equations (1) - (4) all in dBm scale. This method is possible as the output is continuously monitored by the final detection step and the Brillouin amplifiers must be updated multiple times per input time step in order to time-multiplex the values of the A matrix. While the elements of the A and B matrices are fixed constants, the amplifier gains and VOA losses are adjusted in each instance to convert the equations from dBm units into physically realizable gain and loss values.

As an example, if we have a specific input to output relation for this matrix multiplication given by $s_i = A_{ij}x_j$, where x_j is -1 dBm and we wish to multiply $A_{ij} = 2$, we would set our Brillouin gain to no gain, and set the VOA to attenuate the signal in order to achieve an output s_i of -2 dBm. If the input x_i is $+1$ dBm and we

wish to multiply still the same value $A_{ij} = 2$, we would set the Brillouin gain to amplify the signal to make $s_i = +2$ dBm. The gain and attenuation values are calculated as Gain or Loss = $10\log_{10}(\frac{P_{\text{out}}}{P_{\text{in}}})$. We can control the Brillouin gain by appropriately tuning the pump power, as explained above. In this way we are able to time multiplex the construction of the A matrix by continuously monitoring the input and varying the VOA attenuation and Brillouin gain accordingly.

At first glance, this might seem like a limitation. However, the conversion from matrix elements in dBm scale to actual hardware parameters is straightforward and does not significantly increase implementation difficulty. We have accounted for this in simulations as well, as is discussed further in Section IV. This also requires the SBS process to respond quickly enough to modulations of the pump. The realistic gain modulation speed of fiber Brillouin amplifiers by modulating the pump power is typically limited to tens of MHz (e.g., up to around 50–100 MHz in silica fibers). This limitation arises from the intrinsic response time of the SBS process, which is governed by the phonon lifetime (approximately 10 ns) or equivalently the Brillouin gain linewidth (50–100 MHz). For example, recent advances in optical imaging [27] have made use of the quick response time of Brillouin amplifiers by modulating at over 1 MHz. Modulating the pump amplitude faster than the limit set by the Brillouin gain linewidth would not allow the acoustic wave (phonons) to fully respond, resulting in reduced or ineffective gain modulation. This tradeoff is discussed further below.

The output from this matrix multiplication on the current sub-step is passed through a compensatory Brillouin amplifier to account for any losses during previous and successive fiber splitting and combining steps, and to pre-amplify the signal before the activation step. It is then passed to the nonlinear activation. The input to the activation function Brillouin amplifier must be used

in a self-pumping scheme [22]. The previous amplification step allows for it to have sufficient power to pump the nonlinear interaction, giving a nonlinear function at the output as shown in Figure 1. Here, we also choose the ratio between the pump and input beams (the pump splitting ratio) appropriately to optimize the nonlinear shape of the activation function, which is expanded on in the next section.

The output is the m 'th element of the state of the reservoir at the next time step, $k + 1$. It is switched into the appropriate output branch by a $1 : N$ switch and the output is given an appropriate delay and split before both being sent to a detector and back into the reservoir for the next time step. This design utilizes only a single nonlinear activation element, allowing for high scalability. After the necessary delays to line up all of the output vectors, and at the end of all of the sub-steps, the state vector has been successfully updated and fed back into the reservoir for the next time step. After collecting all of the state vectors in the detection steps, we use post-training according to Equation (2) to achieve the required estimated output in response to the time-series inputs u_k .

This design allows for the choice of arbitrary matrix elements for the matrix A and vector B , including negative elements in dBm units through the use of the appropriate attenuation before each Brillouin amplifier. If chosen according to the convergence properties of an ESN, this design can be used to implement an arbitrary ESN, which is a universal family of reservoir computers [17]. This means that given a desired accuracy for a task (such as prediction), this method can be used to realize an optical hardware that achieves that accuracy. The proposed design also allows for scalability, as the number of nodes is increased simply by increasing the number of parallel fibers running in the optical fiber reservoir. Although, scalability is naturally limited by available resources and energy.

An important consideration is the energy consumption of the system. While an arbitrary ESN can be implemented with this architecture, the power flowing through the system can approach unfeasible amounts. In order to limit this, the scaling criteria on the amplifiers and nonlinear activation is made stringent to ensure that the maximum value of x_k in the system is 31 dBm. The maximum pump power for the nonlinear activation required in this scenario is 3.2 W for a pump splitting ratio of 1000. The pump splitting ratio is discussed further in Section IV. While this results in a slight degradation in performance, we must accept this tradeoff to keep the power budget low.

Another important trade-off is between scalability and speed of operation involved. The current approach uses time multiplexing to simplify the hardware requirements and allows us to implement the nonlinear activation with only a single module. This is also limited by the response speed of the Brillouin amplifiers to the modulation of pump power, as discussed above. Commercial-off-the-

shelf electro-optic modulators (EOMs) can modulate in the tens of GHz range, allowing for quick response time of optical power variation. If we assume a 1 MHz relatively slow modulation speed for an EOM, this implies an increase in delay of $1 \mu\text{s}$ for every node. While this does cause a slow down in operation speed due to the time multiplexed architecture, without this compromise the hardware requirements grow in complexity and become difficult to scale, requiring N^2 linear Brillouin amplifiers and N nonlinear modules. The time-multiplexing approach also allows access of negative elements through programming of VOAs before each Brillouin amplifier. Thus, we suggest to allow for a reduced speed of operation to ensure a scalable and relatively simpler hardware design. Alternatively, the architecture can be modified to fix the gain of the Brillouin amplifiers, with appropriate attenuation beforehand to always maintain convergence. This will result in a fixed reservoir implementation, but will no longer represent an ESN as the A matrix will change at every time step due to a lack of correction for the input optical power. However, this comes at the cost of the guarantee of universal applicability for an ESN, therefore we have decided against this approach despite the relative hardware simplicity.

The delay line solution adds a different kind of hardware complexity despite reducing the required number of Brillouin amplifiers. While this is a drawback of using a fiber-based approach, we consider this fiber-based architecture to be a preliminary step towards an on-chip all optical architecture. Choudhary et al. [28], and Yu et al. [29] have shown > 50 dB of Brillouin amplifier gain in photonic chip and > 8 dB of gain in thin-film lithium niobate solutions respectively, showing promise that a high-gain and tunable Brillouin amplifier for the construction of a similar on-chip optical ESN may be feasible in the near future. In addition, the on-chip photonic-circuit implementation will allow multiple nonlinear activating Brillouin amplifiers in parallel, obviating the need for delay lines. This future photonic-circuit implementation will ensure the scalability of the machine size.

On-chip implementations will also simplify the phase locking requirement. These systems have much lower phase fluctuations than fiber systems due to the solid on-chip structure, and approaches to combine coherent beams in Silicon On Insulator (SOI) fabrications, such as the method demonstrated by Jiao et al. [30], show promise for this ESN technology to be brought to an on-chip architecture.

IV. RESULTS AND DISCUSSION

The optical ESN architecture was tested in simulation assuming N computational nodes, which refer to N elements of the x_k vector. The number of nodes was varied during testing, which is expanded on below. The performance of our optical ESN was also compared with a similar ESN implemented with code in Python,

using a sigmoid activation function. This comparison is intended to validate our optical ESN, not to show that one approach is superior to the other. Good performance in machine learning hinges on the ability to approximate nonlinear input–output relationships and capture complex temporal dynamics. According to the Stone–Weierstrass theorem [31], the polynomial algebra property is central to achieving universality. Therefore, we selected three distinct tasks to evaluate these critical capabilities. They are the sine-square classification test, prediction of the NARMA10 system, and the Mackey–Glass time series prediction. Each task evaluates mainly the reservoir computer nonlinearity, polynomial algebra capabilities, and dynamic memory retention, respectively. Additionally, we address the nonlinear properties of the SBS interaction and, thus, the optimization of the activation function. To achieve good results in the tasks mentioned above, we require strong enough nonlinearity, while maintaining the convergence conditions of the ESN. We vary the value of the gL product as well as the pump splitting ratio with these constraints in mind to optimize the performance of the ESN in the selected benchmark tests.

To evaluate the performance of the ESN, we use the normalized mean-square error (NMSE) given by

$$\text{NMSE} = \frac{1}{\sigma_y^2} \langle (y - \hat{y})^2 \rangle = \frac{1}{N\sigma_y^2} \sum_{k=0}^{N-1} (y - \hat{y})^2. \quad (8)$$

Here, we average over N time steps to represent the training interval. The estimated output \hat{y}_k is given by Equation (2). Here, σ_y^2 is the variance of the output y . So, this bounds the NMSE by the variance of y . This quantity will be within the interval $(0, 1)$ for the training data set, although it may exceed 1 for an arbitrary data set.

For each test, we analyze the effect of the nonlinear strength of the SBS interaction, given by the gL product value of the medium and the pump splitting ratio for the self-pumped nonlinear activation element, which refers to the ratio of the pump power to the input power. Here, g represents the Brillouin gain and L represents the interaction length. These values appear in Equation (7). The gL product decides the nonlinear shape and the parking point of the activation function, as shown in Figure 1. The pump splitting ratio independently changes the parking point of the activation function, which allows us to optimize it for greater performance. It is important to note however that increasing the splitting ratio increases the power budget of the system. The parking point of the tunable activation function moves between -5 dBm to -10 dBm for the range of gL values that we have used for testing in this work, as shown in Figure 1. This means that, around the parking points, the pump power will be 100–300 mW for a splitting ratio of 1000. Since we have allowed for a maximum output x_k value of 31 dBm, the maximum pump power required in this scenario is 3.2 W, which is quite a feasible power budget for the nonlinear activation elements. Better performance can generally

be achieved for larger splitting ratios, which means that the best performance is restricted by the energy availability. We also evaluate the performance as the number of nodes N is increased, which shows the effect of scaling the ESN. These behaviors are task-dependent and the exact values of these parameters are subject to change with randomization of the ESN and inputs but, by extracting a range of top-performing parameters across the board, we attempt to design the most generally applicable SBS activation function and optical ESN. We do this by analyzing the behavior for 250 trials of different A and B matrices. These investigations are expanded on below.

In order to simulate the proposed architecture for the matrix-vector multiplication, the data at the input and output is always represented in dBm units, which allows access to negative elements as discussed in the previous section. However, the input dBm data is always converted to W units before the multiplication step. This must be done in order to accurately simulate the behavior of optical components such as VOAs and Brillouin amplifiers. The output is converted back to dBm for the detection phase, ensuring that the data is always represented in dBm units.

A. Sine Square Classification

This test is a time series classification task, commonly used in estimating the nonlinearity of computing reservoirs [32]. The input given is a series of randomly arranged sine and square waves, each 8 steps long. The task given to the ESN is to classify the current wave as sine or square. This test helps us understand the nonlinearity of the ESN. Distinguishing between smoothly varying sine waves and abruptly changing square waves requires mapping the data into a higher-dimensional hyperspace (i.e., nonlinear transformation), making classification easier. The results are shown in Figure 3.

On average, we see similar performance in terms of the NMSE with the software ESN using a sigmoid activation performing marginally better. We emphasize that the comparison between the software ESN and the all-optical ESN is not intended to show that one approach is superior to the other. Rather, the comparison serves as a validation check for the numerical simulations of our all-optical ESN. We anticipate that the performance of the software ESN and the all-optical ESN will be quite similar, as both implementations rely on the same underlying model, differing only slightly in their nonlinear activation functions. The reported values for this instance given in the figures are 0.14 for the software ESN and 0.12 for the optical ESN. These are median values from multiple computations.

We evaluate the effect of varying activation function parameters on the NMSE for this test. We have computed the average NMSE over 250 variations of the A and B matrices to see clear trends in the NMSE. From Figures 4 (a) and (b), NMSE decreases consistently with increas-

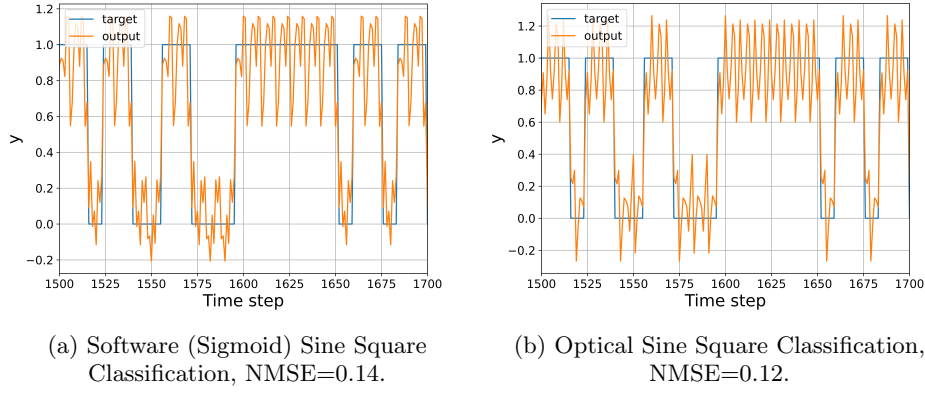


FIG. 3: Comparison of the performance of the Sine-Square Classification test. Parameters: $N = 10$, $gL = 12$, Pump/Input = 1500

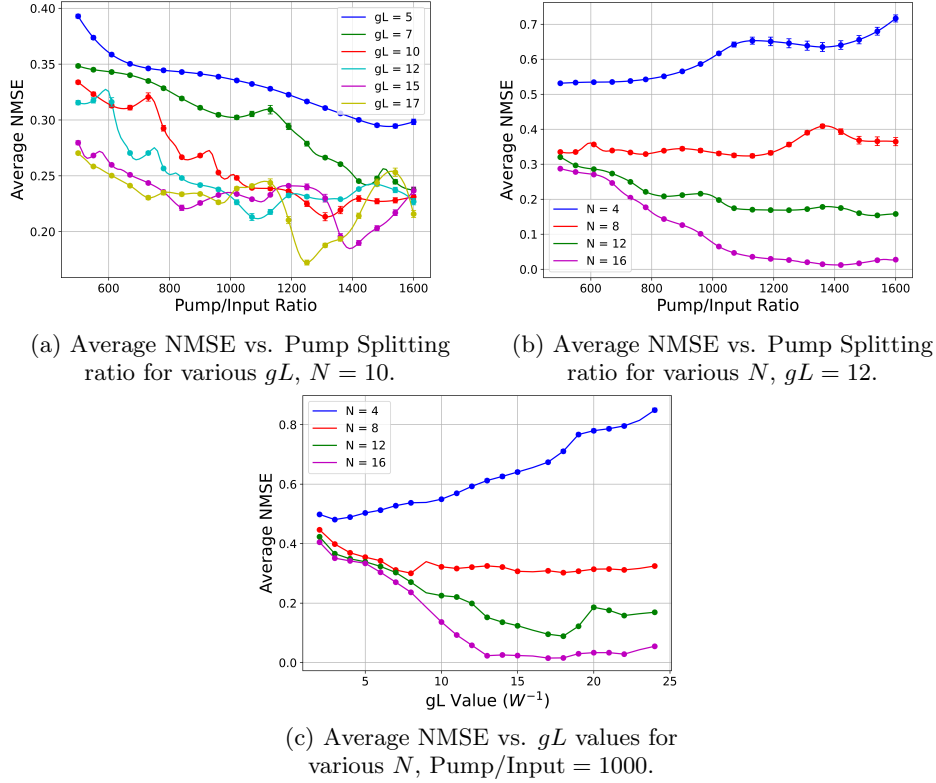
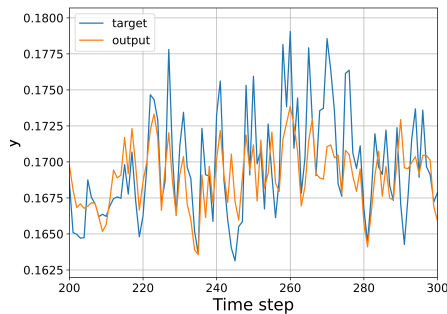


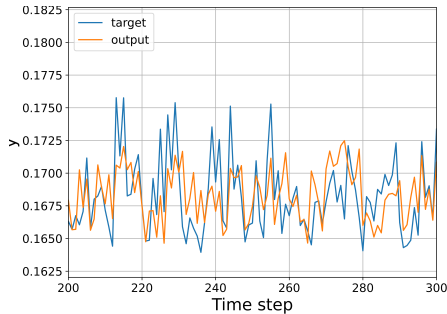
FIG. 4: NMSE vs activation function parameters for the sine square classification test.

ing pump splitting ratios, indicating improved nonlinear activation efficiency. Figure 4 (c) shows that for a fixed pump splitting ratio as well, the performance nearly saturates at lower N values for gL products in the range of $3 - 7 W^{-1}$, with slight (< 0.2) improvements in NMSE for higher gL values in the case of larger N values. We see that for $N = 4$ nodes, the trends are difficult to see and the NMSE values are much higher. This is because the fitting is difficult for a smaller number of nodes. Therefore, we find for this task that $N = 5$ and above are required for reasonable performance, with an increase in N taking the performance closer and closer to saturation

near $NMSE \approx 0$. We also see, from Figure 4 (a) that there is a different optimum point in the performance for each gL value. The most probable reasoning for this behavior is that both the pump splitting ratio and the gL value are together responsible for the optimal parking point of the activation function, resulting in local minima. The values reported by Slinkov et. al [22] allow the possibility of gL values from $3 - 7$ with fiber lengths of $3 - 6$ m at reasonable threshold powers of 1.26 W which are very practical lengths of fiber. Experimental demonstrations have shown much higher levels of nonlinearity in the right materials [28, 33]. This shows promise for the



(a) Software (Sigmoid) NARMA Test, NMSE = 0.57.



(b) Optical NARMA Test, NMSE = 0.54.

FIG. 5: Comparison of the performance of the NARMA10 test. Parameters: $N = 10$, $gL = 12$, Pump/Input = 1500

translation of this architecture into an on-chip implementation, which has the benefit of improved scalability while maintaining the other advantages of this fiber-based approach.

B. NARMA10

Next, the nonlinear autoregressive moving average (NARMA) [34] task is used to test the ESN. This task mainly focuses on the polynomial algebra property of the all-optical ESN reservoir. The model for NARMA10, a version of NARMA popularly used for testing reservoir computers, is given by

$$y_{k+1} = \alpha y_k + \beta y_k \sum_{r=0}^9 y_{k-r} + \gamma u_k u_{k-9} + \delta, \quad (9)$$

$$u_k = \mu + \kappa \Gamma_k, \quad (10)$$

where y_k is the output at time step k for input u_k . We have used values for the constant parameters $(\alpha, \beta, \gamma, \delta) = (0.3, 0.05, 1.5, 0.1)$ and Γ_k is a random variable that takes values from the interval $[-1, 1]$. We have used $\mu = 0$ and $\kappa = 0.1$. This y_k given by Equations (9) and (10) gives us the target sequence that we fit the ESN estimated output to. This is a tenth-order equation with a large time delay of 10 steps, making it a difficult problem. It demonstrates the capability of the reservoir computer to estimate polynomials given random inputs. The results for a software-based ESN are used to evaluate the performance of the optical ESN.

For this test, we used the following parameters of the all-optical ESN: $N = 10$, $gL = 12$, and the pump/input ratio of 1500. On average we see marginally better performance from the software sigmoid ESN, but the NMSE values are comparable. We note that the performance difference between the software and all-optical ESNs arises primarily from differences in their nonlinear activation functions, as all other components are accurately implemented in both systems. In the instance shown in Figure

5, we see an NMSE of 0.57 from the software ESN and 0.54 from the optical ESN. These are median values from multiple computations, and are quite close. This means that our optical ESN performs nearly as good as the theoretical software ideal for the same size of 10 nodes in this particular benchmark, which is a strong result.

Figure 6 shows the behavior of the ESN for this test with varying gL and pump splitting ratio. This test is seen to prefer higher splitting ratios and higher gL values, although the improvement is very slight. These results imply that a stronger pump might be better for the most general applicability of the ESN, which is corroborated by the other tests as well. The minimal variation in NMSE versus the ESN parameters when compared to the other tasks is most likely attributed to the difficulty of the NARMA10 test, which involves inputs sampled from noise. These NMSE values likely represent the saturated values achievable by the optical ESN.

C. Mackey-Glass

Finally, we use the Mackey-Glass task to test the performance of the ESN against the software-based version. This test particularly focuses on the dynamic memory retention capability of the all-optical ESN. This test requires an approximation of the Mackey-Glass chaotic time series equation [35] given by

$$\frac{dy}{dt}(t) = \beta \frac{y(t-\tau)}{1 + y^n(t-\tau)} - \gamma y(t). \quad (11)$$

The values chosen for the constants in Equation (11) are the standard values $(\beta, \tau, n, \gamma) = (0.2, 17, 10, 0.1)$. The solution to this equation is numerically approximated and allowed to run for 1000 steps before being used for the task. The task given to the ESN is to predict 5 steps ahead of the input, i.e. given the input $u_k = y_{k-5}$ we want a successful prediction of y_k . This benchmark evaluates the reservoir computer's memory capacity and its ability to predict chaotic temporal variations. Strong

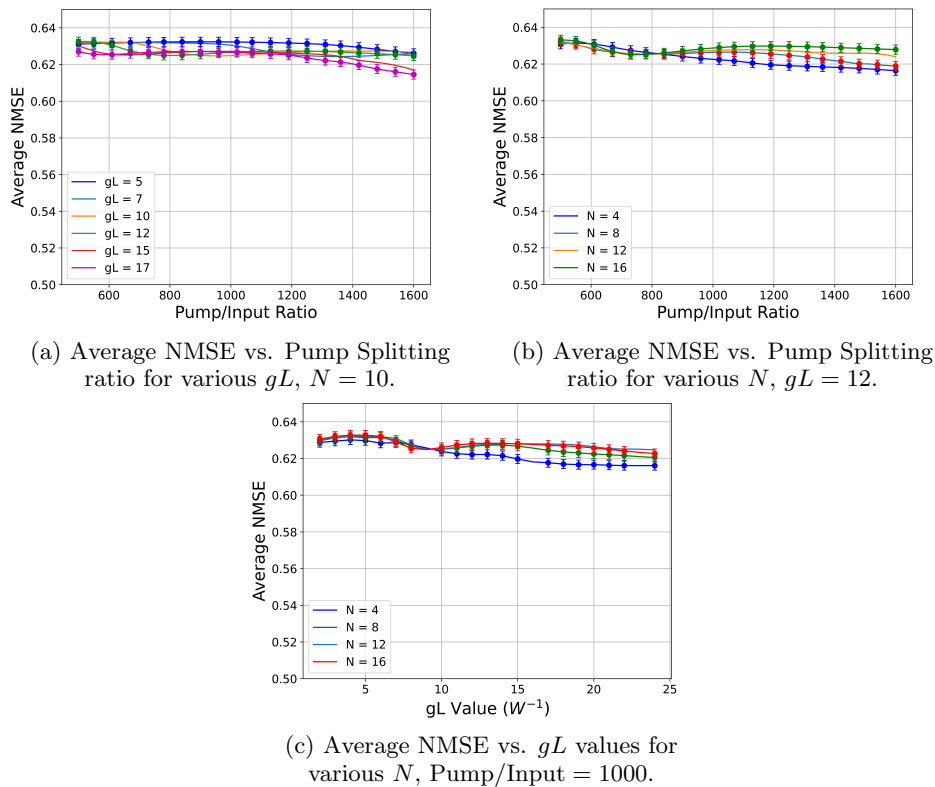


FIG. 6: NMSE vs activation function parameters for the NARMA10 test.

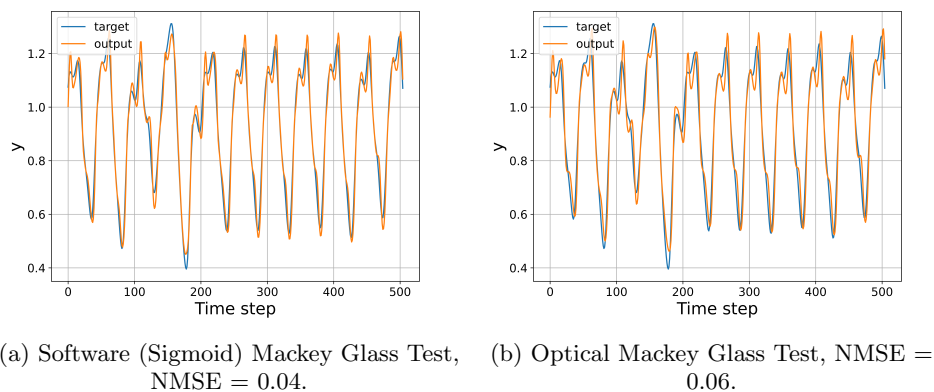


FIG. 7: Comparison of the performance of the Mackey-Glass time series prediction test. Parameters: $N = 10$, $gL = 12$, Pump/Input = 1500

performance in this test indicates that the optical reservoir has sufficient long-term memory for effective time-based predictions, as accurately forecasting future values of a complex analytical time-series requires robust extrapolation capabilities derived from effective dynamic memory retention. We evaluate the same benchmark in the software-based sigmoid ESN, and compare the two to estimate the theoretical fit of the optical ESN. We used the following parameters for the all-optical ESN: $N = 10$, $gL = 12$, and a pump/input ratio of 1500. For this test as well, on average we see marginally better performance from the software ESN, with the NMSE

reported for the instance shown in Figure 7 as 0.04 for the software ESN and 0.06 for the optical ESN. These NMSE values are median values seen from multiple trials. These results demonstrate that the optical ESN achieves competitive accuracy using a compact 10-node architecture, underscoring its practicality for resource-constrained applications.

Figure 8 shows the behavior with the variation of pump splitting ratio and gL value. Similar to the results from the sine square classification test, the NMSE decreases with larger pump splitting ratio and shows improper fitting for $N = 4$. Although, the variation in values is slight

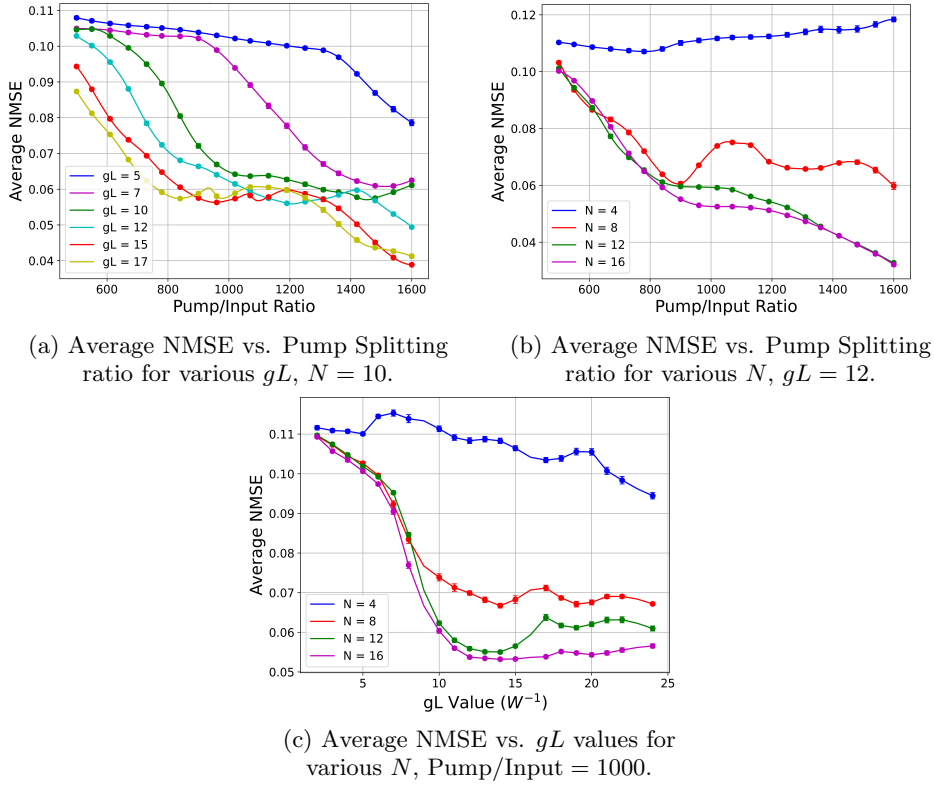


FIG. 8: NMSE vs activation function parameters for the Mackey-Glass test.

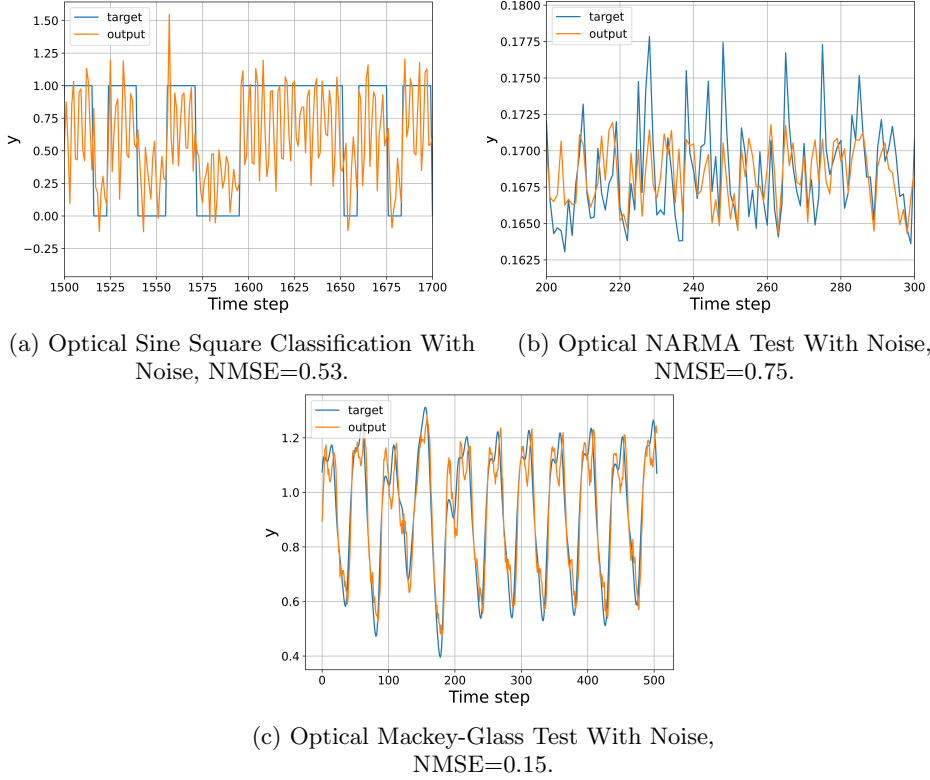


FIG. 9: Examples of Test Performance in the Presence of Detection Noise

here as well, similar to the NARMA10 test. Across all tests, it seems that a high pump splitting ratio and a gL

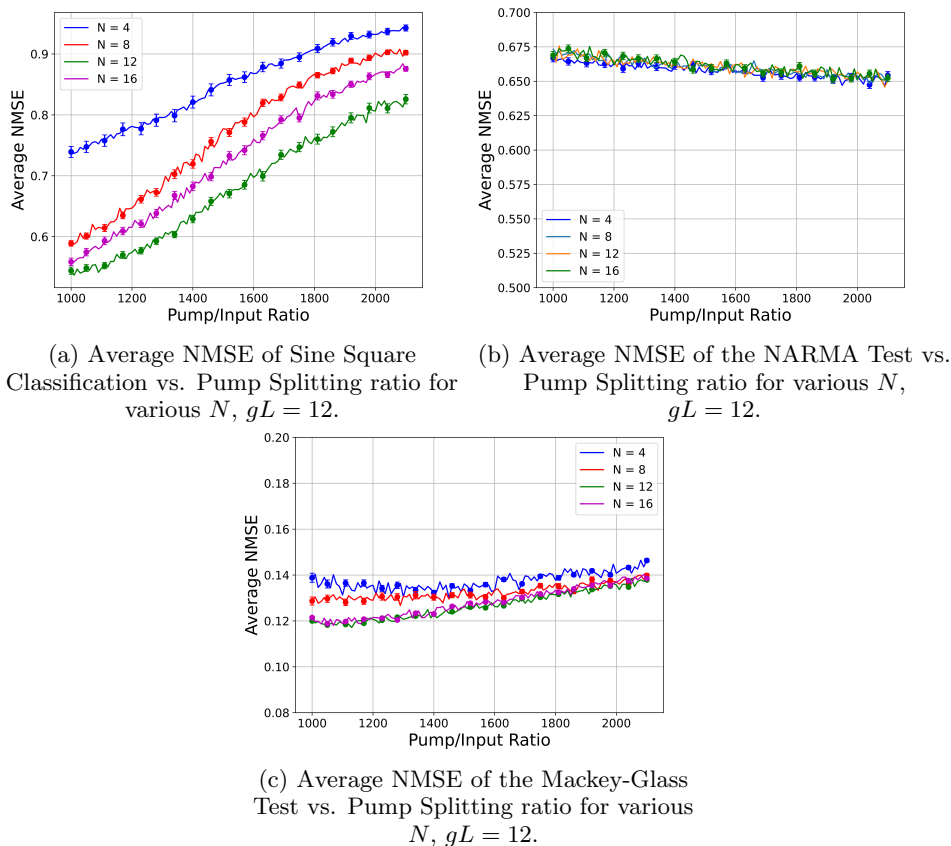


FIG. 10: Performance of Benchmark Tests in the Presence of Detection Noise

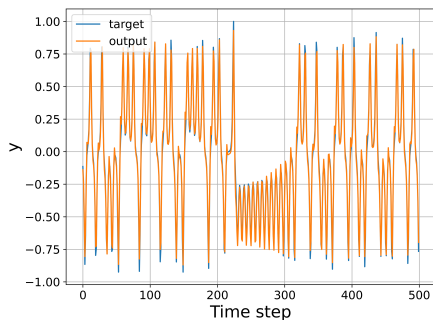
value of around $5 - 10 W^{-1}$ can ensure the best results, as the improvement from further increasing the gL value is marginal at the cost of increased hardware complexity. While these behaviors can vary between tests and randomization, ensuring good performance across all three tests ensures good performance for the optical ESN in general application. In order to limit the energy consumption of the system, the pump splitting ratio can be limited to 1000. This still shows good results, as can be seen from Figures 4, 6, and 8. While a larger pump splitting ratio is generally more beneficial to performance, we accept the slight degradation in exchange for enhanced feasibility of the system through a smaller pump power budget.

D. Noise Performance and Negative Values

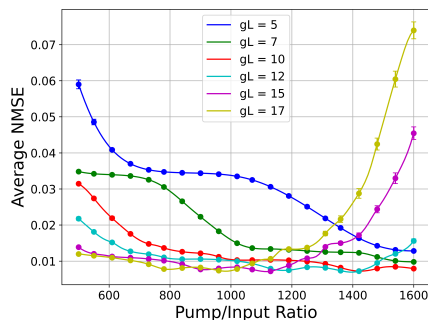
For the case of a weak input probe undergoing high gain amplification, Brillouin amplification is known to be noisy [36]. This noise scales with pump intensity and is more prominent in cases with pump beam aberration, which can cause reduced performance by the optical reservoir [37]. In our design, these intense gain values are not necessary for the matrix multiplication steps, making our reservoir relatively safe from high gain noise. To fur-

ther reduce the impact, the amplified spontaneous noise (ASE) can be mitigated by the use of a band-pass filter [22] and in our simulations, we see good performance without requiring output probe powers over 31 dBm, which would result in a negligible noise level. Another source of noise is optical power detection noise. This is accounted for by a simple gaussian noise model. Figure 9 shows examples of the performance of the optical ESN with detector noise included, compared with Figures 3, 5, and 7. For this test, we assumed the noise property of 0.32% uncertainty at 1550nm wavelength, which is a standard treatment of considering detector noise [38]. In the presence of noise, the nonlinear capability is severely reduced as can be seen in the sine-square classification test results. This is mitigated by choosing an optimal gL value with a large pump splitting ratio, as detailed in the previous section. We observe from Figure 10 that the average NMSE begins to trend upward, unlike the noise free cases of Figures 4, 6, and 8. The cause of this is likely that the saturation point for the specific task as a function of pump/input ratio is reached earlier because of the presence of detection noise.

The optical ESN shows robustness in its time-series prediction ability, even in the presence of noise. The reported median NMSE in Figure 10 for the Mackey-Glass test is 0.15. This shows that the long-term memory capability is not diminished by the presence of noise, al-



(a) Optical Lorenz System Test.
NMSE=0.018



(b) Variation of Lorenz System Test NMSE
with Pump Splitting Ratio

FIG. 11: Lorenz-X Prediction Results to Demonstrate Accessibility of Negative Values

though there is a plateau in performance with varying pump splitting ratio, as can be seen from Figure 10 (c). We can see that overall, after accounting for power detection noise in the fiber setup, there is a reduction in performance of around 0.1 – 0.5 NMSE with more reduction in the classification task and less effect on prediction, implying that the efficiency of nonlinearity is affected more by the noise than the long and short term memory capabilities of the optical reservoir. These noise properties are for commercially available optical detectors. Hence, the negative impact of noise on performance can be further mitigated with the use of low noise detectors [39], [40].

One drawback of the selected benchmark tests is that they do not cover negative values. In order to demonstrate the ability of our design to access and predict negative inputs and targets, we use the Lorenz system test. It involves predicting the x-coordinate of a chaotic time series function [41]. The results for this test are shown in Figure 11.

We can see in Figure 11 that the architecture is able to produce negative outputs, and performs well for a task that involves negative values as well as positive values. We also see similar conclusions from the performance in this task as the other three: a gL value of $5 - 10W^{-1}$ is preferred and stronger pump splitting ratios provide better performance. This shows that negative values are also accessible for this architecture by using dBm units for the optical power.

V. CONCLUSION

We have provided the design for a feasible all-optical ESN with minimal resource overhead and energy requirements. For the nonlinear activation and matrix multiplication, we use SBS in two regimes: the large pump regime for linear behavior, and the self-pumped regime for nonlinear behavior. In the linear regime, tuning the pump power along with required attenuation using VOAs is enough to achieve the necessary multiplications. For the

nonlinear activation step, according to reported achievable values of Brillouin gain in highly nonlinear fibers (HNLFs) [22], our design requires a fiber of length 3 – 6 m to achieve the required nonlinearity for good results, which is a very practical length of fiber. Such fibers also have a reasonable threshold power to show the required nonlinear output.

Additionally, our design requires only a single Brillouin fiber amplifier as a nonlinear activation device, making it highly scalable. However, a trade-off in computation speed has been introduced to allow for this scalable design. It is possible to achieve faster operation speeds at the cost of scalability, but this also greatly increases the hardware resource requirement, so we have decided against this approach. The nonlinear activation is optimizable by tuning the gL value of the SBS amplifier as well as the pump splitting ratio, which refers to the ratio of the pump to the input given to the self-pumped Brillouin amplifier. By doing so, we analyze the behavior of the optical ESN for multiple benchmark tests to find the most optimal activation function design, while ensuring low overall energy consumption.

Our matrix multiplication and beam combination steps make use of standard fiber optical components such as VOAs, fiber beam combiners, 1:N splitters, combiners, and a 1:N switch. We see comparable results to a standard software ESN using a sigmoid activation function. To show this, we chose three tasks: classification of sine and square waves, prediction of the NARMA10 sequence, and prediction of the Mackey-Glass chaotic time series. Each benchmark task demonstrates the nonlinearity, polynomial algebra capability, and long-term memory of this ESN respectively, showing that universal computations are indeed accessible with this hardware. We validated our numerical simulations of the designed all-optical ESNs by comparing them to a software ESN with a sigmoid activation function. The results demonstrated that both systems achieve similar performance when using an equal number of nodes. This shows the feasibility and effectiveness of an all-optical approach to building an ESN.

VI. ACKNOWLEDGMENT

This material is based upon work supported by the U.S. Department of Energy, Office of Science, Office

of Biological and Environmental Research under Award Number DE-SC0025910.

-
- [1] S. Hochreiter and J. Schmidhuber, *Neural computation* **9**, 1735 (1997).
- [2] M. Yan, C. Huang, P. Bienstman, P. Tino, W. Lin, and J. Sun, *Nature Communications* **15**, p.2056 (2024).
- [3] D. J. Gauthier, E. Bollt, A. Griffith, and W. A. Barbosa, *Nature communications* **12**, 1 (2021).
- [4] J. Pathak, B. Hunt, M. Girvan, Z. Lu, and E. Ott, *Physical review letters* **120**, p.024102 (2018).
- [5] P.-R. Vlachas, J. Pathak, B. R. Hunt, T. P. Sapsis, M. Girvan, E. Ott, and P. Koumoutsakos, *Neural Networks* **126**, 191 (2020).
- [6] R. S. Zimmermann and U. Parlitz, *Chaos: An Interdisciplinary Journal of Nonlinear Science* **28** (2018).
- [7] D. Canaday, A. Griffith, and D. J. Gauthier, *Chaos: An Interdisciplinary Journal of Nonlinear Science* **28** (2018).
- [8] D. Wang, Y. Nie, G. Hu, H. K. Tsang, and C. Huang, *Nature Communications* **15**, p.10841 (2024).
- [9] P. J. Ehlers, H. I. Nurdin, and D. Soh, *Nature Communications* **16**, 1 (2025).
- [10] P. J. Ehlers, H. I. Nurdin, and D. Soh, *Neural Networks* **184**, 107101 (2025).
- [11] C. Zhu, P. J. Ehlers, H. I. Nurdin, and D. Soh, *arXiv preprint arXiv:2405.04799* (2024).
- [12] C. Zhu, P. J. Ehlers, H. I. Nurdin, and D. Soh, *arXiv preprint arXiv:2412.17817* (2024).
- [13] B. J. Shastri, A. N. Tait, T. Ferreira de Lima, W. H. Pernice, H. Bhaskaran, C. D. Wright, and P. R. Prucnal, *Nature Photonics* **15**, 102 (2021).
- [14] T. Wang, S.-Y. Ma, L. G. Wright, T. Onodera, B. C. Richard, and P. L. McMahon, *Nature Communications* **13**, p.123 (2022).
- [15] S. Phang, *Optics Express* **31**, 22061 (2023).
- [16] F. Dupont, B. Schneider, A. Smerieri, M. Haelterman, and S. Massar, *Optics express* **20**, 22783 (2012).
- [17] L. Grigoryeva and J.-P. Ortega, *Neural Networks* **108**, 495 (2018).
- [18] H. Jaeger, Bonn, Germany: German National Research Center for Information Technology GMD Technical Report **148**, p.13 (2001).
- [19] H. Zhou, J. Dong, J. Cheng, W. Dong, C. Huang, Y. Shen, Q. Zhang, M. Gu, C. Qian, H. Chen, *et al.*, *Light: Science & Applications* **11**, p.30 (2022).
- [20] X. Xu, M. Tan, B. Corcoran, J. Wu, A. Boes, T. G. Nguyen, S. T. Chu, B. E. Little, D. G. Hicks, R. Morandotti, *et al.*, *Nature* **589**, 44 (2021).
- [21] L. Yang, L. Zhang, and R. Ji, in *Optics and Photonics for Information Processing Vii*, Vol. 8855 (SPIE, 2013) pp. 100–104.
- [22] G. Slinkov, S. Becker, D. Englund, and B. Stiller, *arXiv preprint arXiv:2401.05135* (2024).
- [23] S. Boyd and L. Chua, *IEEE Transactions on circuits and systems* **32**, 1150 (1985).
- [24] P. J. Ehlers, H. I. Nurdin, and D. Soh, *arXiv preprint arXiv:2312.15141* (2023).
- [25] R. W. Boyd, A. L. Gaeta, and E. Giese, *Springer Handbook of Atomic, Molecular, and Optical Physics* (Springer, 2008) pp. 1097–1110.
- [26] W. Liang, N. Satyan, F. Aflatouni, A. Yariv, A. Ke-witsch, G. Rakuljic, and H. Hashemi, *Journal of the Optical Society of America B* **24**, 2930 (2007).
- [27] R. Shaashoua, L. Kasuker, M. Kishner, T. Levy, B. Rotblat, A. Ben-Zvi, and A. Bilenca, *Nature Photonics* **18**, 836 (2024).
- [28] A. Choudhary, B. Morrison, I. Aryanfar, S. Shahnia, M. Pagani, Y. Liu, K. Vu, S. Madden, D. Marpaung, and B. J. Eggleton, *Journal of lightwave technology* **35**, 846 (2016).
- [29] S. Yu, R. Zhou, G. Yang, Q. Zhang, H. Zhu, Y. Yang, X.-B. Xu, B. Chen, C.-L. Zou, and J. Lu, *Laser & Photonics Reviews* , 2500027 (2025).
- [30] S. Jiao, J. Qiu, J. Song, K. Xu, Y. He, G. Yuan, W. Guo, Y. Li, and J. Wu, in *CLEO: Applications and Technology* (Optica Publishing Group, 2024) pp. JTh2A–104.
- [31] M. H. Stone, *Mathematics Magazine* **21**, 237 (1948).
- [32] J. Dudas, B. Carles, E. Plouet, F. A. Mizrahi, J. Grollier, and D. Marković, *npj Quantum Information* **9**, p.64 (2023).
- [33] B. J. Eggleton, C. G. Poulton, P. T. Rakich, M. J. Steel, and G. Bahl, *Nature Photonics* **13**, 664 (2019).
- [34] A. F. Atiya and A. G. Parlos, *IEEE transactions on neural networks* **11**, 697 (2000).
- [35] M. C. Mackey and L. Glass, *Science* **197**, 287 (1977).
- [36] A. Scott, D. E. Watkins, and P. Tapster, *JOSA B* **7**, 929 (1990).
- [37] C. Nathe, C. Pappu, N. A. Mecholsky, J. Hart, T. Carroll, and F. Sorrentino, *Chaos: An Interdisciplinary Journal of Nonlinear Science* **33** (2023).
- [38] I. Vayshenker, X. Li, D. J. Livigni, T. R. Scott, and C. L. Cromer, *Optical fiber power meter calibrations at NIST* (NIST, 2000).
- [39] Q. Lu, Q. Shen, Y. Cao, S. Liao, and C. Peng, *IEEE Transactions on Nuclear Science* **66**, 1048 (2018).
- [40] K. Gasmı, *Optical Engineering* **55**, 097101 (2016).
- [41] E. N. Lorenz, *Journal of atmospheric sciences* **20**, 130 (1963).

Appendix A: SBS Transcendental Equation Derivation

This section provides the derivation to the transcendental Equation (7) which was numerically solved to simulate the behavior of the SBS activation function. Starting from Equations (5) and (6)

$$\frac{dP_p}{dz} = \frac{dP_s}{dz} \implies P_p(z) = P_s(z) + C. \quad (\text{A1})$$

We can write the integration constant as

$$C = P_p(L) - P_s(L) = P_p - P_{\text{out}}, \quad (\text{A2})$$

where we define $P_s(L) = P_{\text{out}}$. We also define $P_s(0) = P_{\text{in}}$. Here, L is the length of SBS interaction. It follows from Equation (6) that

$$\frac{dP_s}{P_s(P_s + P_p - P_{\text{out}})} = -gdz. \quad (\text{A3})$$

This can be formally integrated as

$$\int_{P_s(0)}^{P_s(z)} \frac{dP_s}{P_s(P_s + P_p - P_{\text{out}})} = - \int_0^z gdz'. \quad (\text{A4})$$

$$\implies \ln \left(\frac{P_s(z)(P_{\text{in}} + P_p - P_{\text{out}})}{P_{\text{in}}(P_s(z) + P_p - P_{\text{out}})} \right) = -gCz. \quad (\text{A5})$$

This can be rewritten as

$$\begin{aligned} P_s(z)(P_{\text{in}} + P_p - P_{\text{out}}) - P_{\text{in}}P_p e^{-(P_p - P_{\text{out}})gz} \\ = (P_s(z)P_{\text{in}} - P_{\text{out}}P_{\text{in}})e^{-(P_p - P_{\text{out}})gz}. \end{aligned} \quad (\text{A6})$$

If we substitute $z = L$ and use $P_s(L) = P_{\text{out}}$, we get a transcendental equation in terms of P_{out}

$$P_{\text{out}}(P_{\text{in}} + P_p - P_{\text{out}}) - P_{\text{in}}P_p e^{-(P_p - P_{\text{out}})gL} = 0. \quad (\text{A7})$$

This is the required final result.